International Journal of Microwave and Wireless Technologies

cambridge.org/mrf

Design and fabrication of optically transparent transmitarrays using inkjet-printing technology

Han Chang, Fei-Peng Lai and Yen-Sheng Chen

Department of Electronic Engineering, National Taipei University of Technology, Taipei, Taiwan

Research Paper

Cite this article: Chang H, Lai FP, Chen YS (2024) Design and fabrication of optically transparent transmitarrays using inkjet-printing technology. *International Journal of Microwave and Wireless Technologies* **16**(7), 1162–1172. https://doi.org/10.1017/S1759078724000497

Received: 21 January 2024
Revised: 24 March 2024
Accepted: 5 April 2024

Keywords:
additive manufacturing; inkjet-printing; millimeter wave; transmitarray antennas; transparent antennas

Corresponding author: Yen-Sheng Chen; Email: yschen@ntut.edu.tw

Abstract

This paper explores the use of inkjet-printing technology for transparent transmitarrays, presenting a viable alternative to traditional copper microwire counterparts. The study focuses on achieving high-gain performance crucial for wireless communication systems, with a particular emphasis on the fifth-generation (5G) millimeter-wave communication. Transparent transmitarrays leverage transparent conducting films and conductive mesh structures, overcoming opacity limitations and seamlessly integrating with urban architecture. In this paper, the inkjet-printing process is detailed for fabricating transmitarray apertures, highlighting the flexibility and precision in depositing nanosilver particles onto a glass substrate. The design intricacies involve optimizing feeding characteristics, determining unit cell structures, and constructing transmitarrays of various sizes. To validate the proposed technique, three different apertures (15×15, 20×20, and 25×25 unit cells) are constructed. The antenna performances are evaluated in terms of reflection coefficients, radiation efficiency, realized gain, and patterns, demonstrating the effectiveness of inkjet-printed transmitarrays. Comparative analysis with copper microwire counterparts is also conducted, validating the inkjet-printing technology for similar gain performance with added advantages of flexibility, compatibility with transparent substrates, and cost-effective manufacturing.

Introduction

In contemporary antenna design, achieving high gain is crucial for enhancing the performance of wireless communication systems. Antenna arrays are commonly used for gain improvements, often requiring complex feed networks and substantial dimensions. While traditional methods involve curved reflectors or lens with intricate three-dimensional (3D) manufacturing processes, the planar counterparts, including reflectarrays and transmitarrays, serve as a more accessible alternative. Utilizing planar substrates and printed circuit board (PCB) techniques streamlines the fabrication process, providing an efficient high-gain solution.

The introduction of transparent transmitarrays revolutionizes high-gain antenna design. Overcoming opacity limitations, the transmitarrays seamlessly integrate with urban architecture, including transparent surfaces like windows and facades. Preserving spatial efficiency, transparent transmitarrays offer inconspicuous deployments, addressing challenges posed by traditional high-gain techniques. Their transparent nature allows deployment on various surfaces, promoting efficient the fifth-generation (5G) millimeter-wave communication without compromising aesthetics.

Transparent transmitarrays leverage two main types of conductors: Transparent conducting films (TCFs) [1–9] and conductive mesh structures [10–16]. TCFs such as indium tin oxide (ITO) achieve transparency due to their plasma frequency within the visible light spectrum. Materials including fluorine-doped tin oxide, aluminum-doped zinc oxide, and gallium-doped zinc oxide offer alternatives, and stacking multiple layers is explored. On the other hand, mesh structures void high-conductivity materials periodically, suitable for transparent antennas.

Initially developed for satellites, transparent reflectarrays optimize space utilization by integrating optically transparent structures with solar modules [1]. Studies on transparent film conductors predominantly feature ITO, ensuring high optical transparency in high-frequency applications. In contrast, investigations into mesh conductors commonly involve highly conductive metals such as copper, offering versatility in frequency applications. In this study, the exploration of the conductivity trade-off leans toward microwires for their superior conductivity over TCFs, while simultaneously leveraging inkjet-printing to simplify the intricate manufacturing process.

This paper serves as a significant contribution to the advancement of transparent antenna technologies. The motivation is to demonstrate the feasibility and effectiveness of inkjet-printed transparent transmitarrays for 5G millimeter-wave communication. Through the design,

fabrication, and analysis of transparent transmitarrays using inkjet-printing technology, we present an alternative to the conventional use of copper microwires. While transparent antennas have historically relied on copper, the utilization of copper microwires has limitations on etching process, high costs, and limited scalability associated with achieving high resolution, whereas inkjet-printing offers a cost-effective, scalable, and flexible alternative with comparable performance. By undertaking a comparative analysis between inkjet-printed transmitarrays and their counterparts fabricated using copper micromesh [16]. This study aims to unveil the advantages and viability of inkjet-printing for transparent transmitarrays, specifically targeting applications in modern wireless communications [17–20].

Inkjet-printing process

Before delving into the detailed design of the transmitarray, this section provides essential background information on the fabrication process, emphasizing the implementation of inkjet-printing technology. In comparison to traditional etching methods commonly used in PCB technology, inkjet-printing stands out for its unparalleled flexibility in depositing conductive material onto substrates. This technology excels in printing complex and highly precise graphical structures, making it adaptable to flexible substrates. Furthermore, it facilitates the deposition of multiple layers of materials and intricate antenna encapsulation techniques.

Surface tension testing of the substrate precedes the inkjet-printing process, ensuring optimal adhesion of the ink. In this study, DGP 40LT-15C nanosilver particle ink, with a conductivity of 10^7 S/m and a surface tension of 35–38 dyn/cm, was employed. The chosen glass substrate, based on its surface tension compatibility, demonstrated ink adhesion during the dyne pen test, with a surface tension value of 38 dyn/cm.

Confirmation of compatibility between the ink and substrate surface tension is followed by the calibration of the 16 printhead positions in the inkjet cartridge. The setting of droplet ejection speed takes into consideration potential printhead clogs, which could adversely affect droplet ejection stability and, consequently, the quality of printed patterns. With the substrate securely in place on the nanomaterial inkjet-printing platform, a vacuum process is initiated to stabilize the substrate and ensure printing precision. This study employed a Fujifilm Dimatix DMP-2850 nanomaterial printer for its flexibility in applications, including the printing of structures on flexible substrates and the deposition of multiple material layers.

The subsequent curing process is crucial for solidifying the nanosilver particles on the printed substrate. A heat gun, specifically the SIGMA BS400 Oven, is employed for gradual temperature increases, preventing uneven volatilization and the occurrence of the coffee-ring effect – a phenomenon associated with inconsistent evaporation rates of conductive ink. The heating process is applied by increasing the temperature every 10 minutes until reaching a temperature elevation of 30°C, and maintained at the curing temperature of nanosilver particles for 40 minutes. Finally, the inkjet-printing process is completed with the curing of nanosilver particles on the printed substrate, ensuring uniformity and minimizing the potential for issues such as the coffee-ring effect.

Antenna design

The proposed inkjet-printed transparent transmitarray design employs an array of unit cells on a transparent substrate to manipulate the phase of incident electromagnetic waves. Each unit cell introduces a specific phase delay based on its physical dimensions and electromagnetic properties. Through strategic variation of phase delays, constructive interference is achieved, enabling efficient beam steering. The unit cell geometry and configuration are optimized to ensure uniform phase distribution, facilitating precise control over the transmitted wave front. This approach enables effective beam steering and radiation pattern control, suitable for diverse wireless communication applications.

Feed

In the design of transmitarrays, the effective utilization of the radiation field of a feeding antenna to generate coherent interference is crucial. The choice of a feed antenna often involves selecting one with a high front-to-back ratio (FBR) to avoid backward radiation. Figure 1 shows the quasi-Yagi antenna serving as the feed, fabricating on a 0.2 mm thick Rogers RO4003 substrate with a relative permittivity (ε_r) of 3.55. In simulated patterns at 28 GHz, the quasi-Yagi antenna exhibits an FBR value of 20.2 dB, indicating a high FBR suitable for the transmitarray. The antenna also demonstrates a bandwidth of 22.1%, covering 25.53–31.54 GHz. The E-plane and H-plane radiation patterns at 28 GHz indicate half-power beam widths (HPBWs) of 57° and 113°, respectively.

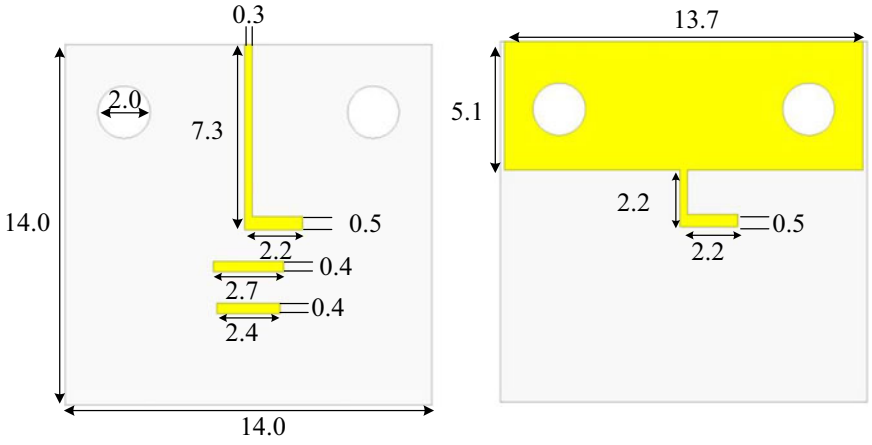

Figure 1. Geometry of the feeding quasi-Yagi antenna (unit: mm).

https://doi.org/10.1017/S1759078724000497 Published online by Cambridge University Press

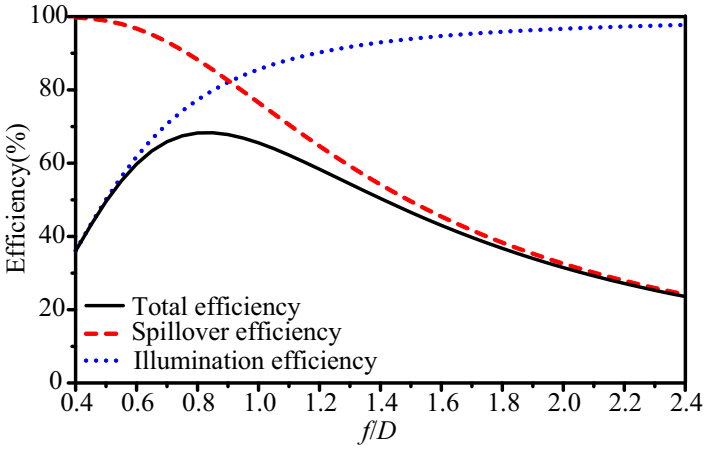

(a)

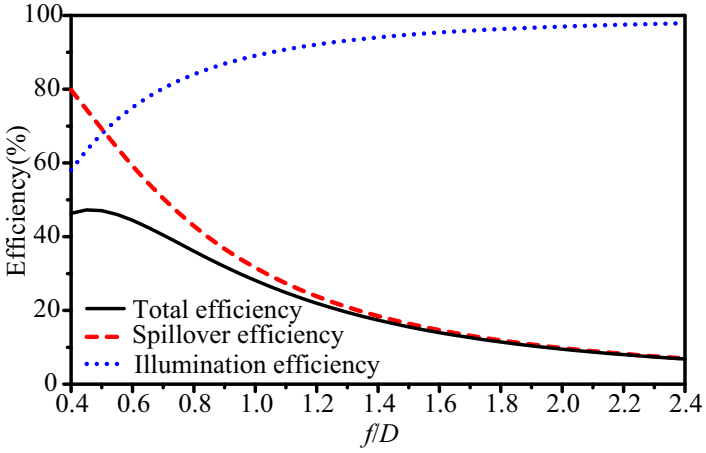

(b)

Figure 2. Analysis of the focal length-to-diameter ratio on the (a) E-plane and (b) H-plane for the feeding quasi-Yagi antenna.

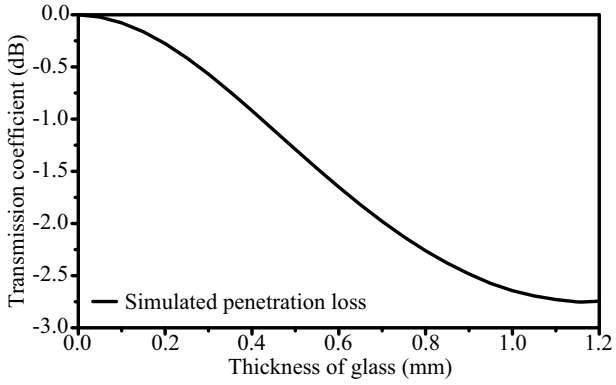

Figure 3. Penetration loss corresponding to different glass thicknesses.

Investigating the HPBWs of the feed antenna holds paramount importance in the design of transmitarrays, influencing the focal distance (f) and subsequently governing the focal length to diameter ratio (f/D). The f/D plays a crucial role in determining how effectively the radiation pattern of the feed antenna illuminates the entire aperture of the transmitarray. In our optimization strategy, we employ the power of cosine functions $\cos^q(\theta)$ to fit the radiation patterns for both E-plane and H-plane, where q represents the power. The quasi-Yagi antenna introduces nonsymmetric radiation patterns in both planes. By determining the optimum q for both planes, we can calculate the illumination efficiency (η_i), spillover efficiency (η_s), and total efficiency (η_t). These efficiencies are expressed as follows:

$$\eta_i = \frac{\left\{\frac{[(1-\cos^{q+1}\theta_e)]}{(q+1)} + \frac{[(1-\cos^{q}\theta_e)]}{q}\right\}^2}{2\tan^2\theta_e\left[\frac{(1-\cos^{2q+1}\theta_e)}{(2q+1)}\right]} \quad (1)$$

$$\eta_s = 1 - cos^{2q+1}\theta_e \quad (2)$$

$$\eta_t = \eta_i \times \eta_s \quad (3)$$

The evaluation of these efficiencies at different f/D values is instrumental in optimizing the design and maximizing the utilization of both the radiation pattern of the feed and the transmitarray aperture. Figure 2 illustrates the results for the E-plane

https://doi.org/10.1017/S1759078724000497 Published online by Cambridge University Press

and H-plane, showcasing the trade-off involved. Notably, the E-plane achieves 68% total efficiency at an f/D of 0.8, while the H-plane reaches 46% total efficiency at an f/D of 0.4. Striking a balance between utilizing the entire glass area and achieving desirable total efficiencies for both E-plane and H-plane, the optimal choice emerges as a square transmitarray design with an f/D of 0.6. This square design facilitates an effective compromise, ensuring efficient utilization of the glass area while achieving the desired total efficiencies in both planes.

Unit cells

After evaluating the characteristics of the feed, the next design mission is the unit cells. This study employs eight distinct structures for the distribution of phase compensation. The discretization of phase compensation into eight unit cells necessitates each unit to possess a phase difference of 45°. For the design of the unit cells, the eight structures utilized must not only satisfy an integer multiple of 45° in phase differences among themselves but also consider the penetration loss incurred during transmission. Therefore, an analysis is conducted on the glass substrate to assess the structural implications of glass thickness, as illustrated in Fig. 3. The analysis reveals that at a glass thickness of 1.0 mm, the incurred penetration loss is approximately 2.6 dB. To enhance the phase tuning range of the designed unit cell, this study ultimately opts for a three-layer metal structure using two glass substrates with $\varepsilon_r = 5.26$ and a thickness of 0.5 mm. This choice aims to achieve a larger phase tuning range while considering the trade-off with penetration loss.

The multilayer structure of the unit cell established from the above analysis is depicted in Fig. 4(a). This structure takes into account the fixed separation between the two glass substrates, namely, 0.01 mm. The next step involves analyzing the amplitude and phase shift variations caused by changing the geometric parameters of the unit cell. The objective is to identify structures that meet the criteria of penetration amplitude attenuation less than 3 dB and possess a phase tuning range of 315°. This analysis aims to explore how alterations in the geometric parameters of the unit cell impact the electromagnetic wave penetration structure.

Based on this profile, five unit cell topologies are developed, as shown in Fig. 4(b). The analysis of the amplitude attenuation and phase variation of the five unit cell structures concerning the length

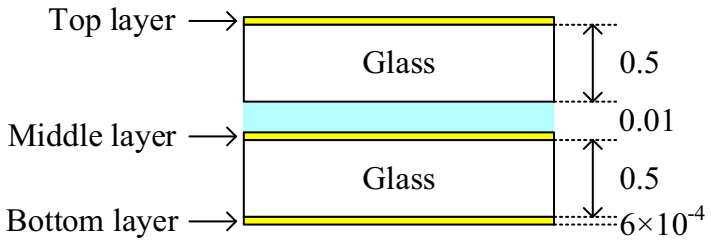

(a)

Configuration	A	B	C	D	E
Illustration					
Top layer					
Middle layer					
Bottem layer					

(b)

Figure 4. (a) Side view, (b) 3D view, and top view of the unit cell (unit: mm).

https://doi.org/10.1017/S1759078724000497 Published online by Cambridge University Press

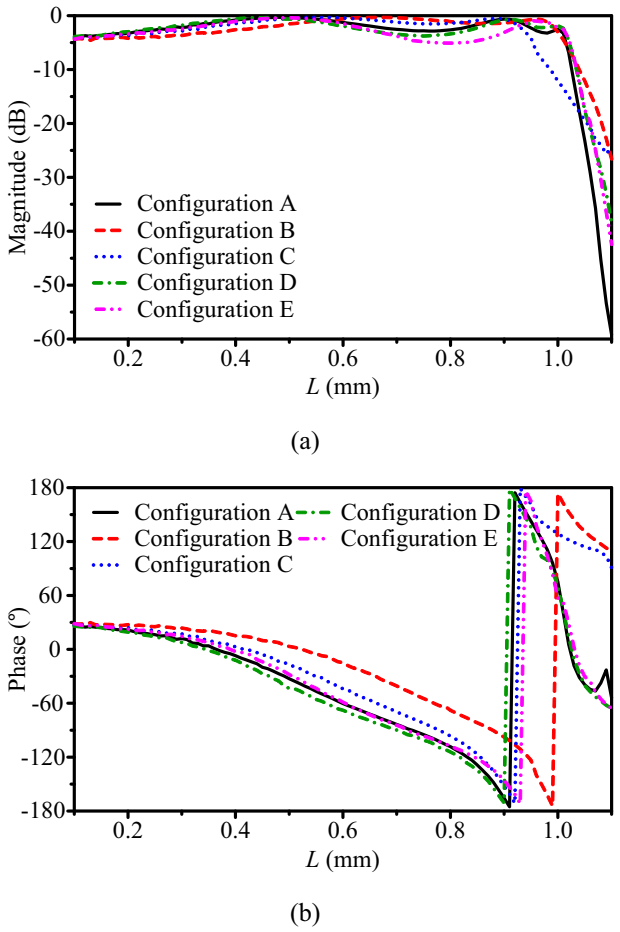

Figure 5. (a) Magnitude and (b) phase of transmitting waves as the function of *L*.

of the bar, denoted by *L*. The transmissive amplitude and phase are characterized and illustrated in Fig. 5.

For Configuration *A*, adjusting *L* can achieve a phase tuning range of 338°. However, Configuration A exhibits penetration losses greater than 3 dB when *L* ranges from 0.97 to 0.99 mm. This results in a significant reduction in the energy of the penetrating wave to half or even less. Additionally, at *L* ranging from 0.99 to 1.01, the phase sensitivity is excessively high. Choosing a structure with high phase sensitivity poses challenges in practical implementation, as it can lead to phase deviations due to fabrication errors, emphasizing the need for multiple structures in the design process.

Configuration *B* achieves a phase tuning range of approximately 205° when *L* ranges from 0.37 to 1.01 mm. Configuration *C* shows similar performance to Configuration *B*, featuring a hollow structure in the middle layer. By adjusting *L*, Configuration *C* achieves a phase tuning range of 209° when *L* ranges from 0.26 to 0.94 mm. Configuration *D* achieves phase tuning ranges of 101° (*L*: 0.20–0.66 mm) and 195° (*L*: 0.82–1.01 mm). Ensuring uniform phase differences among adjacent phase unit cells is crucial in the design of transmitarrays. Finally, Configuration *E* was developed with a phase tuning range of 95° (*L*: 0.24–0.66 mm) and 157° (*L*: 0.66–1.01 mm).

After analyzing unit cell structures for amplitude and phase shift variations using simulation software, eight unit cell structures were selected from the five types to compose the elements of the transmitarray. These structures were numbered based on their role as the phase reference point: Structure with a phase delay of 0° was assigned as Number 1, and structures with phase delays of 45°, 90°, and so forth, were consecutively numbered. The characteristics of unit cell are summarized in Table 1.

Table 1. Characteristics of the eight unit cells

No.	Configuration	*L* (mm)	Transmission coefficient (dB)	Phase (°)
1	*D*	0.97	−2.41	0
2	*A*	0.94	−2.60	42.46
3	*B*	0.99	−2.47	87.28
4	*C*	0.86	−0.74	132.20
5	*B*	0.84	−1.65	179.98
6	*A*	0.50	−0.62	225.01
7	*A*	0.29	−1.83	270.05
8	*E*	1.004	−2.84	330.49

It is worth noting that the proposed design method simplifies the optimization process by focusing on a single design factor (the length of the bar, *L*) and a single objective (phase). This streamlined approach allowed us to systematically tailor the unit cell structures to meet the performance requirements of the transmitarray, preventing the use of multiobjective optimization algorithms.

Transmitarrays

With these unit cells in hand, we can construct the unit cells based on the *f*/*D* identified by "Feed" and the phase distribution requirements for constructive interference. Specifically, when the feed source emits waves at an angle θ_i, and the coordinates of the *i*th unit element are (x_i, y_i), with (θ_b, φ_b) denoting the angle of transmitting beam focusing, k_0 representing the propagation constant in free space, and d_i signifying the distance from the feed source to the *i*th unit element, the phase $\varphi_T(x_i, y_i)$ on the *i*th unit element is determined by

$$\varphi(x_i, y_i) = -k_0 (\sin\theta_b \cos\varphi_b x_i + \sin\theta_b \sin\varphi_b y_i) \quad (4)$$

$$\varphi(x_i, y_i) = -k_0 d_i + \varphi_T(x_i, y_i) \quad (5)$$

$$\varphi_T(x_i, y_i) = k_0 [d_i - (x_i \cos\varphi_b + y_i \sin\varphi_b) \sin\theta_b] \quad (6)$$

where $\varphi(x_i, y_i)$ represents the phase shift introduced at the *i*th unit element, which is computed by the spatial coordinates of the unit element relative to the incident angle of the beam in equation (4). This equation illustrates how the phase shift at each unit element is influenced by its position within the transmitarray structure and the direction of the incident wave front. In equation (5), the term $-k_0 d_i$ accounts for the phase shift due to the propagation distance, while $\varphi_T(x_i, y_i)$ represents the additional phase shift introduced by the unit element itself. This equation captures the combined effect of distance-related phase shifts and element-specific phase contributions, providing an understanding of the total phase shift experienced by each unit element. In equation (6), $\varphi_T(x_i, y_i)$ represents the phase shift attributable solely to the unit element's geometric configuration. The term $d_i - (x_i \cos\varphi_b + y_i \sin\varphi_b) \sin\theta_b$ accounts for the distance-dependent phase shift adjusted by the unit element's spatial orientation relative to the incident beam angle

https://doi.org/10.1017/S1759078724000497 Published online by Cambridge University Press

(θ_b, φ_b). This equation elucidates how the geometric properties of each unit element modulate the phase of incident waves, thereby influencing the overall phase distribution across the transmitarray.

Given the goal of demonstrating the feasibility of the inkjet-printed transparent transmitarray in this paper, we designed three different sizes of transmitarray apertures, including 15 × 15 unit cells (3.5 λ × 3.5 λ), 20 × 20 unit cells (4.6 λ × 4.6 λ), and 25 × 25 unit cells (5.8 λ × 5.8 λ), where λ denotes the wavelength. According to the optimal f/D of 0.6, using the dimensions of these three transmitarrays, we can then determine the focal length (f). Specifically, the phase compensation distributions for the transmitarrays of 15 × 15, 20 × 20, and 25 × 25 unit cells are illustrated in Fig. 6. By assembling the eight numbered unit cells from "Transmitarrays" according to these phase compensation distributions, we obtain the transmitarray apertures, which are also shown in Fig. 6.

Antenna performance

The performance of the three inkjet-printed transparent transmitarrays is evaluated in this section. Photographs of the proposed structure and the experimental setup are shown in Fig. 7. First, we test the measured performance, providing a direct assessment of the accuracy to the design methodology. Subsequently, to underscore the inkjet-printing capability, we compare the measured performance of the inkjet-printed transmitarray with test

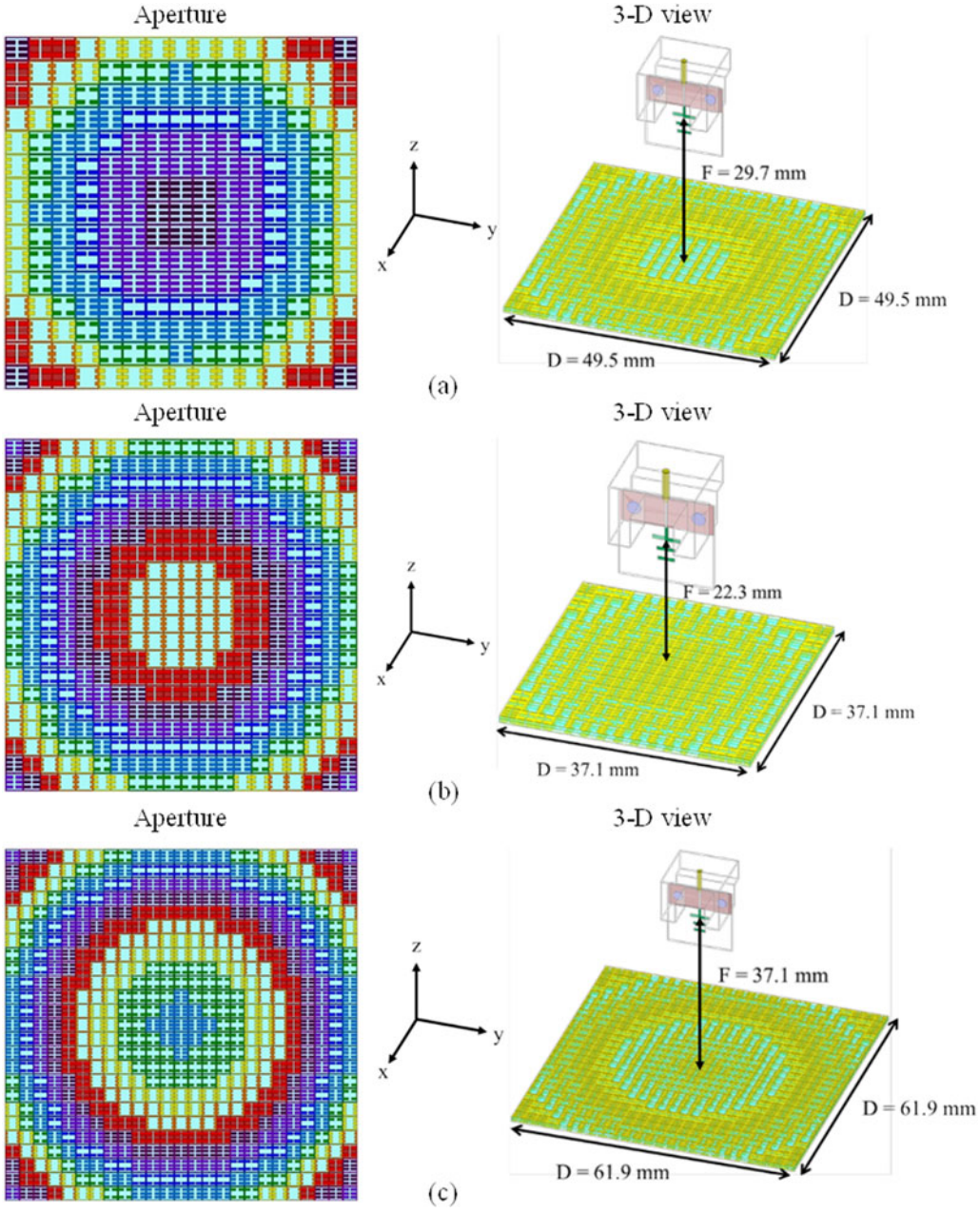

Figure 6. Aperture structure and 3D view of the (a) 15 × 15, (b) 20 × 20, (c) 25 × 25 transparent transmitarrays.

https://doi.org/10.1017/S1759078724000497 Published online by Cambridge University Press

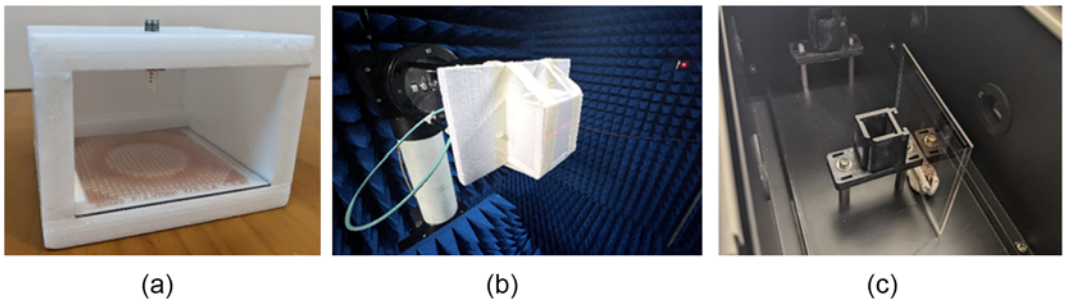

Figure 7. Experimental setup for the proposed transparent. (a) Integrated structure. (b) Measurement of far-field performance in a Compact Antenna Test Range (CATR) anechoic chamber. (c) Measurement of transparency.

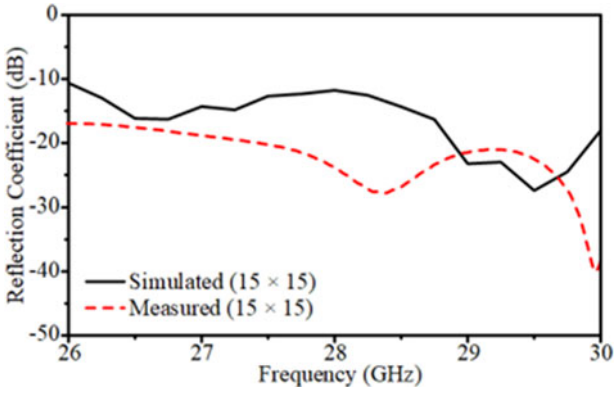

Figure 8. Simulated and measured reflection coefficient of the 15 × 15 inkjet-printed transparent transmitarray.

pieces fabricated using copper microwires through a conventional PCB process. This comparative study aims to elucidate the effectiveness and limitations of inkjet-printing in realizing transmitarrays.

Results

For the 15 × 15 transmitarray, the reflection coefficients across the 27–29 GHz frequency range consistently fall below −10 dB, as shown in Fig. 8. Good impedance matching is achieved for the feed with transmitarray aperture considered. As for the radiation performance, Fig. 9 presents the radiation efficiency and realized gain, showing that measured results are slightly lower than the simulated ones. Figure 10 illustrates the simulated and measured patterns for the E-plane and H-plane at 28 GHz, showing an HPBW of 18.3° (E-plane) and 17.5° (H-plane) along with an FBR value of 12.01 dB. Overall, the measured broadside gain at 28 GHz is 14.87 dBi, indicating sufficient gain enhancement is achieved.

Moving on to the 20 × 20 transmitarray, the reflection coefficients are depicted in Fig. 11, with a decreasing trend toward higher frequencies. At 28 GHz, the simulated and measured reflection coefficients are −16.9 dB and −25.8 dB, respectively. Figure 12 exhibits radiation efficiency and realized gain, where a measured gain of 16.94 dBi is attained. The measured efficiency is slightly lower than the simulated one. Figure 13 shows the simulated and measured two-dimensional (2D) patterns, with an HPBW of 13.1° (E-plane) and 12.4° (H-plane) along with an FBR value of 10.33 dB. The beam width is sharpened and varies as the aperture size.

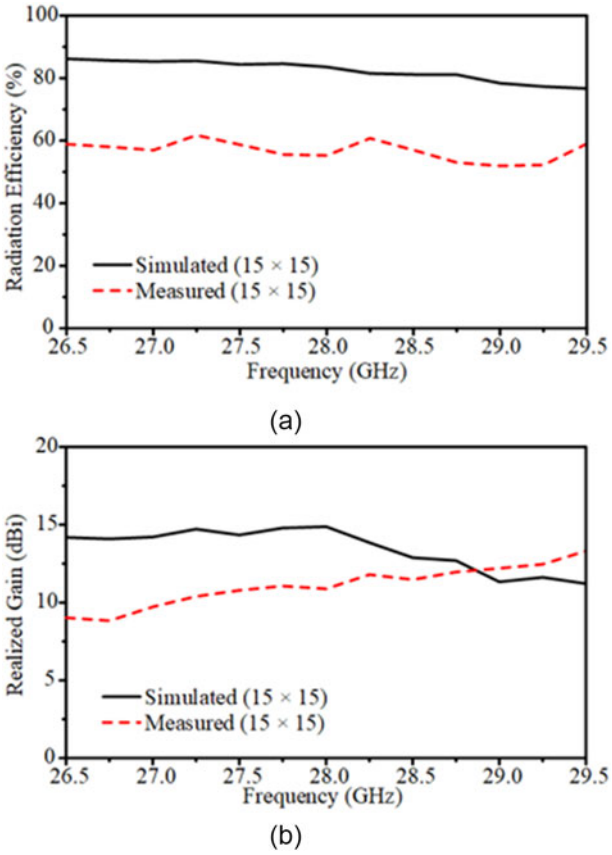

Figure 9. Simulated and measured (a) radiation efficiency and (b) realized broadside gain of the 15 × 15 inkjet-printed transparent transmitarray.

Extending the analysis to the 25 × 25 transmitarray, the reflection coefficients remain consistently below −10 dB within the 26–30 GHz range, as shown in Fig. 14. At 28 GHz, the simulated and measured reflection coefficients are −17.4 dB and −22.4 dB, respectively. The radiation efficiency and realized gain are provided in Fig. 15, and the simulated and measured 2D patterns at 28 GHz are depicted in Fig. 16. The broadside gain becomes 18.82 dBi, featuring an HPBW of 10.8° (E-plane) and 10.0° (H-plane) along with an FBR value of 19.10 dB.

In summary, the measured performance of the inkjet-printed transmitarrays, including 15 × 15, 20 × 20, and 25 × 25 configurations, consistently demonstrates efficient operation with low reflection coefficients, high radiation efficiency, and desirable radiation

https://doi.org/10.1017/S1759078724000497 Published online by Cambridge University Press

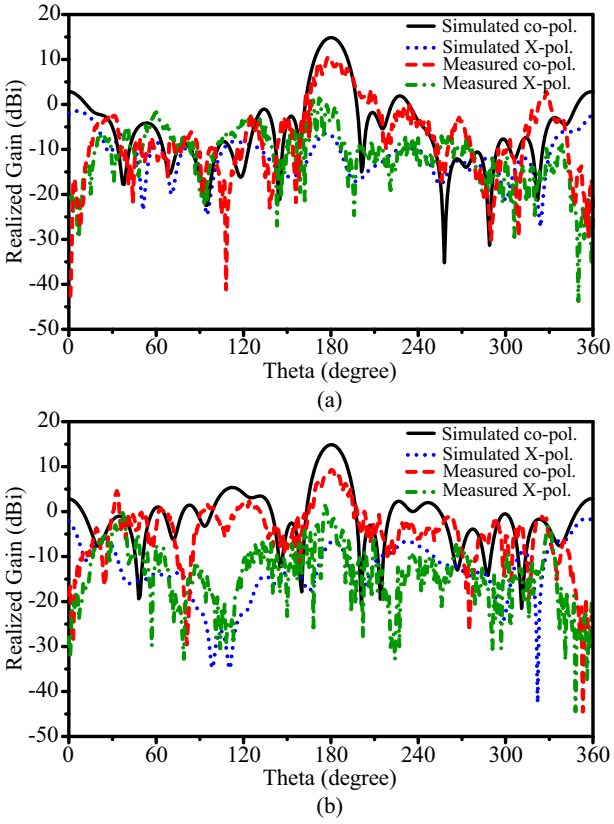

Figure 10. Simulated and measured (a) E-plane and (b) H-plane patterns of the 15 × 15 inkjet-printed transparent transmitarray.

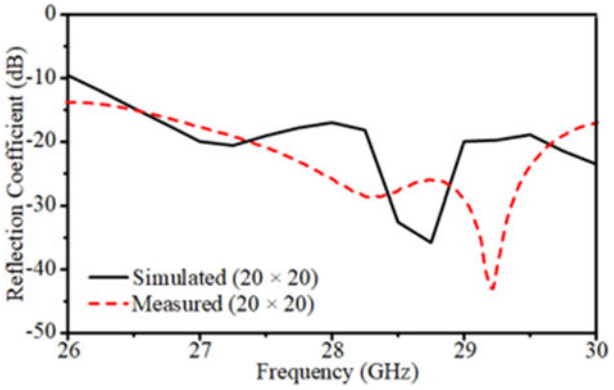

Figure 11. Simulated and measured reflection coefficient of the 20 × 20 inkjet-printed transparent transmitarray.

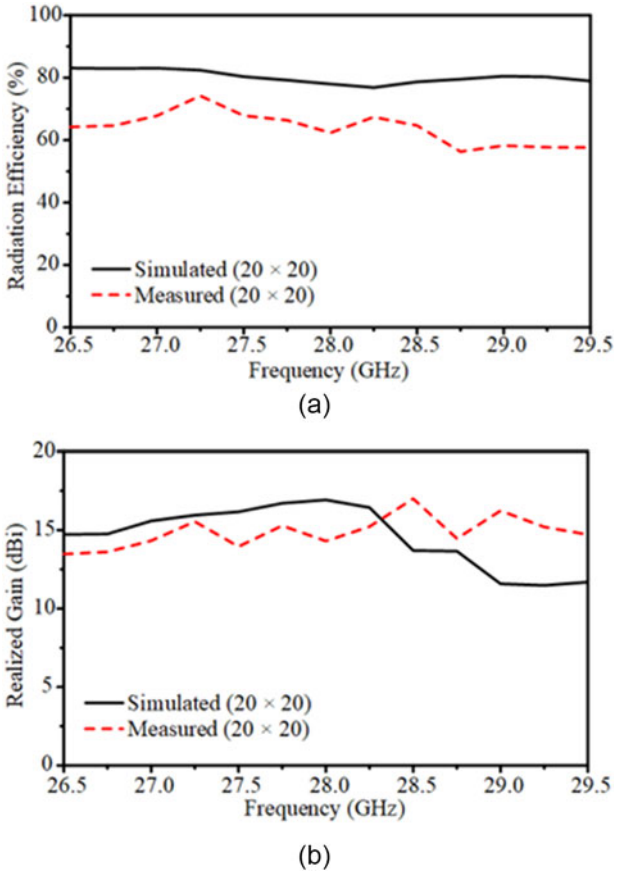

Figure 12. Simulated and measured (a) radiation efficiency and (b) realized broadside gain of the 20 × 20 inkjet-printed transparent transmitarray.

patterns across the specified frequency ranges, confirming the effectiveness of the transparent inkjet-printed technology.

The performance of the proposed inkjet-printed transparent transmitarrays is compared with the state-of-the-art, as shown in Table 2. It illustrates the antenna performance comprising transparent transmitarrays or reflectarrays with different fabrication technology. These apertures exhibit various dimensions with different broadside gains. However, it is noteworthy that among the listed works, the current study stands out as the only one utilizing inkjet-printing technology to fabricate transparent transmitarray apertures. This pioneering approach offers several advantages, including enhanced flexibility, cost-effectiveness, and compatibility with transparent substrates, which are essential for inconspicuous deployments in urban architecture and integration with emerging technologies such as 5G millimeter-wave communication. The proposed structures, characterized by a frequency of 28.0 GHz, aperture dimensions from 3.5 × 3.5 λ^2 to 5.8 × 5.8 λ^2, and broadside gains from 14.9 to 18.8 dBi, demonstrate the efficacy of inkjet-printing with nanosilver particles in achieving high-gain performance for transparent transmitarrays. This comparative analysis underscores the novelty and significance of the current study in advancing transparent antenna technologies and highlights the potential for inkjet-printing to revolutionize the fabrication of high-performance antennas for various applications.

Comparison with copper microwires

Next, we present a comparison of the performance between inkjet-printed and copper microwire transmitarrays across varying sizes. The copper microwire counterparts were designed and fabricated through a conventional PCB process [16].

Beginning with broadside gain and gain enhancement, the inkjet-printed 15 × 15 transmitarray achieves a 14.87 dBi, with a gain enhancement of 7.29 dB. In comparison, the copper microwire counterpart records a gain of 15.11 dBi and a slightly higher gain enhancement of 7.53 dB. Examining the broadside gain for the inkjet-printed 20 × 20 transmitarray, we observe a gain of 16.94 dBi. In comparison, the copper microwire counterpart in the

https://doi.org/10.1017/S1759078724000497 Published online by Cambridge University Press

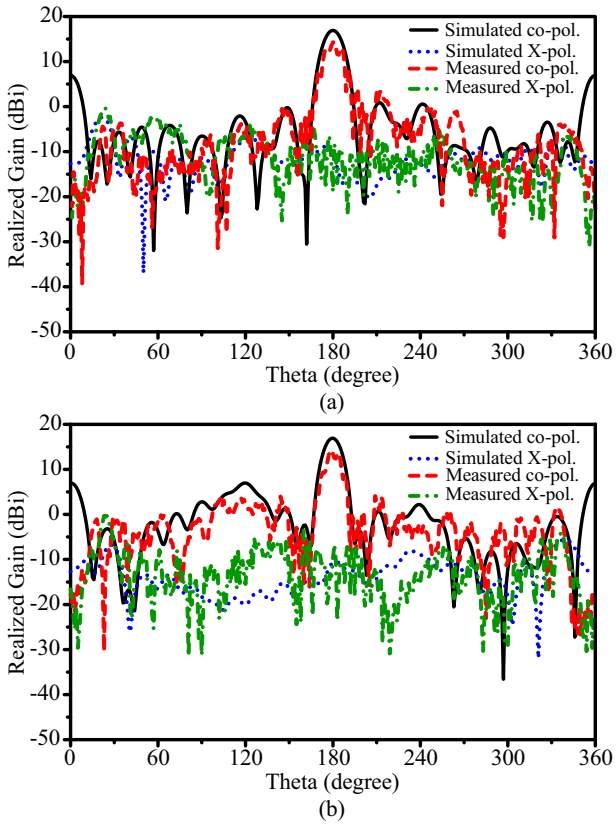

Figure 13. Simulated and measured (a) E-plane and (b) H-plane patterns of the 20 × 20 inkjet-printed transparent transmitarray.

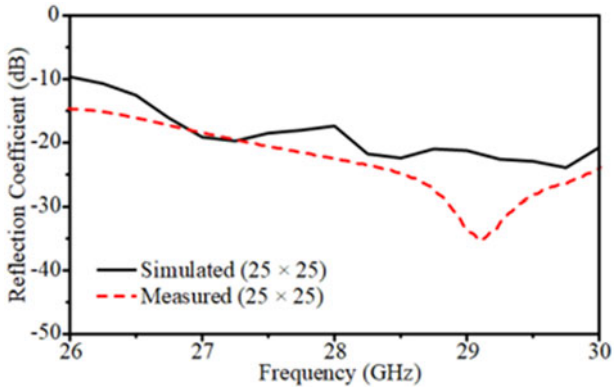

Figure 14. Simulated and measured reflection coefficient of the 25 × 25 inkjet-printed transparent transmitarray.

same size achieves a gain of 16.98 dBi. Scaling up to the 25 × 25 configuration, the inkjet-printed transmitarray demonstrates a gain of 18.82 dBi. On the other hand, the copper microwire counterpart at 25 × 25 showcases a gain of 19.55 dBi.

In terms of radiation efficiency, both inkjet-printed and copper microwire transmitarrays demonstrate high radiation efficiency, with values ranging from 78% to 84% and 80% to 83%, respectively. This suggests that inkjet-printing does not incur extra loss in the manufacturing process.

In summary, the comparative results indicate that the inkjet-printing technology achieves similar antenna gain and additional loss as compared to the PCB process. Also, our results persist

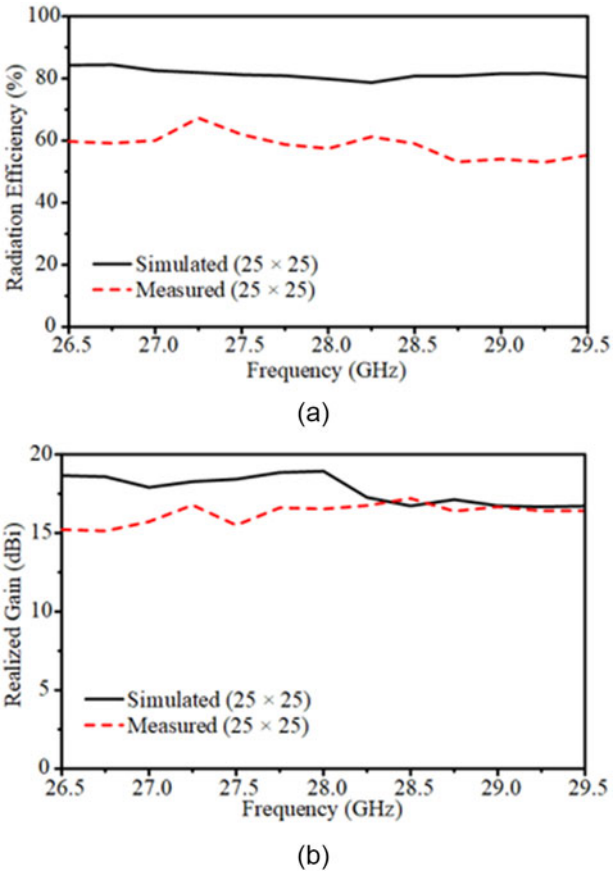

Figure 15. Simulated and measured (a) radiation efficiency and (b) realized broadside gain of the 25 × 25 inkjet-printed transparent transmitarray.

as we scale to larger transmitarrays. This validates the inkjet-printing technology for transparent transmitarrays, enabling additional advantages including flexibility in design, compatibility with transparent substrates, and cost-effective, scalable manufacturing as compared to PCB. These factors contribute to the overall appeal of inkjet-printing technology in the development of transparent electromagnetic devices.

Potential applications

By integrating the proposed transmitarray structures into transparent surfaces, such as windows or glass partitions, within indoor environments, this technique enables the realization of a surfaces capable of manipulating incident electromagnetic waves to enhance signal reception and transmission for nearby base stations. These windows equipped with transparent transmitarrays function as passive beamforming elements, effectively focusing and steering radio frequency signals toward indoor base stations, thereby mitigating signal attenuation, multipath interference, and shadowing effects commonly encountered in indoor environments. By optimizing signal propagation paths and minimizing signal loss, our transparent transmitarray-enhanced windows contribute to significant improvements in signal quality, coverage, and data throughput for indoor base stations, ultimately enhancing the overall performance and reliability of indoor wireless communication networks.

https://doi.org/10.1017/S1759078724000497 Published online by Cambridge University Press

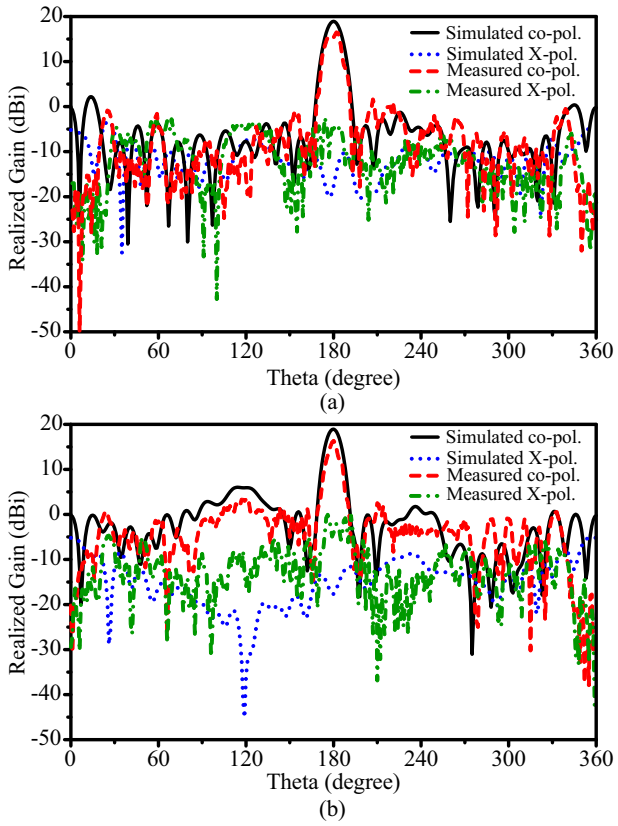

Figure 16. Simulated and measured (a) E-plane and (b) H-plane patterns of the 25 × 25 inkjet-printed transparent transmitarray.

Furthermore, the proposed transparent transmitarrays hold significant promise for applications in augmented reality (AR) and virtual reality (VR) systems. By seamlessly integrating transmitarray functionalities into transparent display panels, the proposed technique empowers AR/VR devices with enhanced imaging capabilities, beam steering, and immersive visual experiences. This integration paves the way for the development of lightweight, high-performance AR glasses and VR headsets, revolutionizing the way users interact with digital content and virtual environments.

Additionally, this study opens avenues for transformative applications in wireless communication networks and satellite communications. The deployment of transparent transmitarrays in satellite antennas enables efficient beamforming, signal focusing, and satellite tracking functionalities, thereby enhancing the performance and reliability of satellite communication systems. Moreover, in terrestrial wireless communication networks, transparent transmitarrays offer opportunities for dynamic beam steering, interference mitigation, and spectrum efficiency improvements, facilitating the deployment of next-generation 5G and beyond-5G networks.

Conclusion

In this paper, we have established inkjet-printing as a promising technology for transparent transmitarrays. The novelty of this paper is fourfold. First, we introduce inkjet-printing as a viable alternative for fabricating transparent transmitarrays, departing from conventional copper microwire techniques. Second, the proposed technique is validated through a comparative analysis, and it achieves comparable performance to their copper microwire counterparts in terms of gain enhancement. Third, this study offers the seamless integration of inkjet-printed transmitarrays with urban architecture. The transparent nature makes the proposed technique ideal for inconspicuous deployments in 5G millimeter-wave communication. Finally, the proposed design overcomes the challenge of the glass substrate through innovative multilayered metal structures, which enhance overall efficiency. The inkjet-printed transmitarrays exhibit robust performance across various sizes, from 15 × 15 to 25 × 25 configurations, showcasing low reflection coefficients, high radiation efficiency, and desirable radiation patterns. The results affirm the viability of inkjet-printing, offering flexibility in design, compatibility with transparent substrates, and cost-effective, scalable manufacturing. This research marks a significant contribution to the advancement of transparent antenna technologies, paving the way for innovative applications in the evolving landscape of wireless communication.

Table 2. Comparisons with transparent reflectarrays or transmitarrays designed at the millimeter-wave band

No.	Type	Frequency (GHz)	Aperture dimensions (λ^2)	Broadside gain (dBi)	Fabrication method
[1]	Reflectarray	25.0	9.2 × 6.7	18.4	PCB (ITO)
[2]	Reflectarray	28.0	9.0 × 9.0	37.2	PCB (ITO)
[3]	Reflectarray	28.0	9.3 × 9.3	30.9	PCB (ITO)
[4]	Reflectarray	26.0	6.6 × 6.6	22.2	PCB (ITO)
[5]	Reflectarray	26.0	4.0 × 4.0	17.1	PCB (ITO)
[9]	Reflectarray	20.0	10.7 × 10.7	27.3	PCB (ITO)
[13]	Transmitarray	28.5	9.9 × 9.9	26.2	PCB (meshed copper)
[14]	Transmitarray	28.5	15.6 × 9.9	25.0	PCB (meshed copper)
[16]	Transmitarray	28.0	67.2 × 67.2	37.5	PCB (meshed copper)
This work	Transmitarray	28.0	3.5 × 3.5	14.9	Inkjet printing (nanosilver particles)
This work	Transmitarray	28.0	4.6 × 4.6	16.9	Inkjet printing (nanosilver particles)
This work	Transmitarray	28.0	5.8 × 5.8	18.8	Inkjet printing (nanosilver particles)

https://doi.org/10.1017/S1759078724000497 Published online by Cambridge University Press

Funding statement. This work was supported by the Ministry of Science and Technology, Taiwan, under Contract MOST 111-2221-E-027-047-MY2.

Competing interests. The authors report no conflict of interest.

References

1. **Chen Y-S, Wu Y-H and Chung C-C** (2020) Solar-powered active integrated antennas backed by a transparent reflectarray for CubeSat applications. *IEEE Access* **8**, 137934–137946.
2. **Peng J-J, Qu S and Xia M** (2020) Optically transparent reflectarray based on indium tin oxide with improved efficiency. *IEEE Transactions on Antennas and Propagation* **68**(4), 3289–3294.
3. **Peng J-J and Qu S** (2019) Single layer optically transparent reflectarray based on indium tin oxide. In *2019 IEEE MTT-S International Wireless Symposium*, Guangzhou, China, May, 1–2.
4. **Kocia C and Hum SV** (2016) Design of an optically transparent reflectarray for solar applications using indium tin oxide. *IEEE Transactions on Antennas and Propagation* **64**(7), 2884–2893.
5. **Kocia C and Hum SV** (2014) Optically transparent reflectarray for satellite applications. In *The 8th European Conference on Antennas and Propagation*, The Hague, Netherlands, April, 1607–1610.
6. **Wang L, Hagiwara H, Rikuta Y, Kobayashi T, Matsuno H, Hayashi T, Ito S and Nakano M** (2021) Experimental investigation of optically transparent dual-polarized reflectarray with suppressed sidelobe level. In *2020 International Symposium on Antennas and Propagation*, Osaka, Japan, January, 407–408.
7. **Dreyer P, Morales-Masis M, Nicolay S, Ballif C and Perruisseau-Carrier J** (2014) Copper and transparent-conductor reflectarray elements on thin-film solar cell panels. *IEEE Transactions on Antennas and Propagation* **62**(7), 3813–3818.
8. **Zainud-Deen SH and Mabrouk AM** (2017) Graphene based metamaterial lens for terahertz applications. In *2017 Japan-Africa Conference on Electronics, Communications and Computers*, Alexandria, Egypt, December, 148–151.
9. **An W, Xiong L, Xu S, Yang F, Fu H and Ma J** (2018) A Ka-band high-efficiency transparent reflectarray antenna integrated with solar cells. *IEEE Access* **6**, 60843–60851.
10. **Yekan T and Baktur R**. (2016) Design of two transparent X band reflectarray antennas integrated on a satellite panel. In *2016 IEEE International Symposium on Antennas and Propagation*, Fajardo, Puerto Rico, June, 1413–1414.
11. **Miao Z-W, Hao Z-C, Wang Y, Jin B-B, Wu J-B and Hong W** (2019) A 400-GHz high-gain quartz-based single layered folded reflectarray antenna for terahertz applications. *IEEE Transactions on Terahertz Science and Technology* **9**(1), 78–88.
12. **Liu Y, Wang H, Liu G and Dong X** (2017) Design of a transparent reflectarray integrated with solar cells using quad-key element. In *2017 Sixth Asia-Pacific Conference on Antennas and Propagation*, Xi'an, China, October, 1–3.
13. **Liu G, Dehghani Kodnoeih MR, Pham KT, Cruz EM, Gonzalez-Ovejero D and Sauleau R** (2019) A millimeter-wave multi-beam transparent transmitarray antenna at Ka-band. *IEEE Antennas and Wireless Propagation Letters* **18**(4), 631–635.
14. **Liu G, Cruz EM, Pham TK, Ovejero DG and Sauleau R** (2018) Low scan loss bifocal Ka-band transparent transmitarray antenna. In *2018 IEEE International Symposium on Antennas and Propagation & USNC/URSI National Radio Science Meeting*, Boston, Massachusetts, July, 1449–1450.
15. **Jiang P, Jiang W and Gong S** (2021) A mesh-type low RCS reflectarray antenna based on spoof surface plasmon polariton. *IEEE Antennas and Wireless Propagation Letters* **20**(2), 224–228.
16. **Chang H, Lai F-P and Chen Y** (2024) Transparent transmitarray antenna with large aperture for significant gain enhancement in millimeter-wave 5G communication networks. *IEEE Antennas and Wireless Propagation Letters* **23**(2), 663–667.
17. **Kumar A** (2024) Substrate integrated waveguide cavity-backed slot antenna with low cross-polarization over the full bandwidth. *Microwave and Optical Technology Letters* **66**(1), 1–7.
18. **Liu S, Wang Y and Guo L** (2024) A low-cost ultrathin metal-only transmitarray antenna at X-band. In *IEEE Antennas and Wireless Propagation Letters*, 1–5.
19. **Kausar S, Kausar A, Hadi MU and Mehrpouyan H** (2024) Multi-beam high gain steerable transmitarray lens for satellite communication and 5G mm-Wave systems. *AEU - International Journal of Electronics and Communications* **173**, 1–10.
20. **Belen MA, Çalışkan A, Koziel S, Pietrenko-Dabrowska A and Mahouti P** (2023) Optimal design of transmitarray antennas via low-cost surrogate modelling. *Scientific Reports* **13**(1), 1–18.

Han Chang was born in Taoyuan, Taiwan, in 1995. He received the B.S. degree in Physics from Fu Jen Catholic University, New Taipei City, in 2017, and the M.S. degree in Electronic Engineering from the National Taipei University of Technology, Taipei, Taiwan, in 2022. He is currently an RF engineer with Wistron NeWeb Corp., Hsinchu, Taiwan. He is responsible for the research and development of 5G small cell, designing RF front-end circuit, and verifying RF performance the product.

Fei-Peng Lai was born in Chiayi, Taiwan. She received the B.S. degree in Electronic Engineering from the National Taipei University of Technology, Taipei, in 2017, where she is currently pursuing the Ph.D. degree in Electronic Engineering. Her current research interests include chipless RFID, high-gain antennas, and wireless communications. She has participated in numerous research projects, including millimeter-wave antenna arrays for radar applications from Micromax International Corp., Taiwan, and chipless RFID development from the Ministry of Science and Technology, Taiwan. She has served on the reviewer board for several IEEE journals.

Yen-Sheng Chen was born in Taichung, Taiwan. He received the B.S. degree in Electrical Engineering and the M.S. and Ph.D. degrees in Communication Engineering from National Taiwan University, Taipei, Taiwan, in 2007, 2009, and 2012, respectively. Since 2013, he has been a Faculty Member with the Department of Electronic Engineering, National Taipei University of Technology (NTUT), Taipei, where he is currently a professor and the Associate Dean of the College of Electrical Engineering and Computer Science (EECS), NTUT. He has participated in a wide range of research projects, including chipless RF identification, transparent antennas and metasurfaces, millimeter-wave antennas and circuits, RF energy harvesting, antenna array failure correction, antennas for body-centric communications, microwave reconfigurable components, and multiobjective optimization techniques. His recent research interests include high-gain antennas, reflectarrays and transmitarrays, chipless sensor networks, transparent antennas, and inkjet-printing technology. Dr. Chen was a recipient of the Outstanding Reviewers Award from the *IEEE Antennas and Wireless Propagation Letters* for the period 2017–2022; the Outstanding Reviewers Award from the *IEEE Transactions on Antennas and Propagation* in 2019–2021; the Future Tech Award from the Ministry of Science and Technology, Taiwan, in 2021; the Outstanding Research Award from NTUT in 2019; the Dr. Shechtman Young Researcher Award from NTUT in 2018; the Outstanding Research Award from the College of EECS, NTUT, in 2018 and 2019, respectively; and the Remarkable Teaching Award from the College of EECS, NTUT, in 2020. He is currently the Associate Editor of the *IEEE Transactions on Antennas and Propagation*, *International Journal of RF and Microwave Computer-Aided Engineering*, and *IEICE Communications Express*. He has served on the editorial/review boards for many technical journals, transactions, proceedings, and letters.

https://doi.org/10.1017/S1759078724000497 Published online by Cambridge University Press